



A quantum mechanical study of water adsorption on the (110) surfaces of rutile SnO₂ and TiO₂: investigating the effects of intermolecular interactions using hybrid-exchange density functional theory

Journal:	<i>Physical Chemistry Chemical Physics</i>
Manuscript ID:	CP-ART-04-2014-001824.R1
Article Type:	Paper
Date Submitted by the Author:	05-Jun-2014
Complete List of Authors:	Patel, Monica; Imperial College London, Department of Chemistry Sanches, Frederico; Imperial College London, Department of Chemistry Mallia, Giuseppe; Imperial College London, Department of Chemistry Harrison, Nicholas; Science & Technology Facilities Council, Computational Science and Engineering Department; Imperial College London, Department of Chemistry

**A quantum mechanical study of water adsorption
on the (110) surfaces of rutile SnO₂ and TiO₂:
investigating the effects of intermolecular interactions
using hybrid-exchange density functional theory**

M. Patel¹, F. F. Sanches¹, G. Mallia¹ and N. M. Harrison^{1,2}

¹*Thomas Young Centre, Department of Chemistry,*

Imperial College London, South Kensington, London, SW7 2AZ, UK

²*STFC Daresbury Laboratory, Daresbury, Warrington, WA4 4AD, UK **

(Dated: June 5, 2014)

Abstract

Periodic hybrid-exchange density functional theory calculations are used to explore the first layer of water at model oxide surfaces, which is an important step for understanding the photocatalytic reactions involved in solar water splitting. By comparing the structure and properties of SnO₂(110) and TiO₂(110) surfaces in contact with water, the effects of structural and electronic differences on the water chemistry are examined. The dissociative adsorption mode at low coverage (1/7 ML) up to monolayer coverage (1 ML) on both SnO₂ and TiO₂(110) surfaces is analysed. To investigate further the intermolecular interactions between adjacent adsorbates, monolayer adsorption on each surface is explored in terms of binding energies and bond lengths. Analysis of the water adsorption geometry and energetics shows that the relative stability of water adsorption on SnO₂(110) is governed largely by the strength of the chemisorption and hydrogen bonds at the surface of the adsorbate-substrate system. However on TiO₂(110), a more complicated scenario of the the first layer of water on its surface arises in which there is an interplay between chemisorption, hydrogen bonding and adsorbate-induced atomic displacements in the surface. Furthermore the projected density of states of each surface in contact with a mixture of adsorbed water molecules and adsorbed hydroxyls is presented and sheds some light on the nature of the crystalline chemical bonds as well as on why adsorbed water has often been reported to be unstable on rutile SnO₂(110).

* monica.patel10@imperial.ac.uk

I. INTRODUCTION

Semiconducting metal oxides are used in a large number of applications, due to their novel and tunable electronic, chemical and mechanical properties. Tin dioxide (SnO_2) and titanium dioxide (TiO_2) are both wide band gap semiconductors that have received considerable attention. SnO_2 is widely used in the sensing of reducing gases [1], hydrocarbon catalysis [2], and as a transparent conductor [3]. TiO_2 has applications in heterogeneous catalysis [4], sorbent technology [5], dye-sensitised solar cells [6], and increasingly in photoelectrochemical water splitting for the production of hydrogen [7]. Water splitting is of current interest as a carbon-free and economically-viable route to hydrogen production; the optimisation of materials would be greatly facilitated by an atomic-level understanding of the reaction mechanisms that occur at the photocatalytic oxide surfaces but this is lacking [8, 9]. A detailed atomistic understanding of (i) water chemistry, (ii) reactive intermediates, and (iii) chemical reactions occurring on metal oxide surfaces could facilitate the design of more efficient systems [10–12]. Understanding the chemical reactions involved relies on a valid description of the structure of the oxide-water interface. This study focuses on the first layer of water at model oxide surfaces and explores which properties of the surface govern the structure of the first water layer.

TiO_2 is a transition metal oxide that adopts a variety of crystal structures, the most abundant ones being rutile and anatase. The (110) surface of rutile TiO_2 is the most stable of the rutile low index surfaces and is considered to be a quintessential model metal oxide system for the study of water chemistry [13]. SnO_2 also adopts the rutile structure. Both materials belong to the $P42/mnm$ tetragonal space group and their unit cells are defined by the lattice vectors and angles $\mathbf{a} = \mathbf{b} \neq \mathbf{c}$ and $\alpha = \beta = \gamma = 90^\circ$, as well as the internal coordinate, u . The rutile structure is characterised by sixfold-coordinated metal ions and threefold-coordinated oxygen ions, forming SnO_6 and TiO_6 octahedra in each case. The key difference between the atomic structure of the two materials is the length of the lattice parameters: SnO_2 has larger \mathbf{a} and \mathbf{c} lattice parameters than TiO_2 , which in turn leads to structural differences at the surface. A comparative study of the surface water chemistry therefore deepens the current understanding of water-water and water-surface interactions and, in turn, may aid the prediction of the structure and properties of oxide-water interfaces.

The rutile $\text{TiO}_2(110)$ surface has been extensively characterised using surface sensitive

techniques such as scanning tunneling microscopy (STM) [14, 15]. The observed images suggest that the unreconstructed (1×1) surface is commonly observed [16], which is characterised by a fivefold-coordinated Ti and a twofold-coordinated bridging O per unit cell. From geometrical considerations (the bridging oxygen ions protrude from the rest of the surface) it is plausible to expect that bright spots in STM images correspond to the bridging oxygens ions. Conversely, the states being imaged are in the conduction band (positive applied bias) which predominantly consists of Ti-3d states, suggesting that the bright spots correspond to the Ti ions at the surface. A combination of theory (using plane-wave pseudopotential methods) and experiment has been used to determine that it is, in fact, electronic structure effects that dominate observed STM images (*i.e.* bright spots are attributed to under-coordinated Ti ions) [15]. Although, this can be reversed at very high tunnelling currents, when the tip is close to the surface [15]. The rutile $\text{SnO}_2(110)$ surface is also considered to be the most stable surface of SnO_2 [17–20]. However, STM and low energy electron diffraction (LEED) studies have shown that a number of reconstructions can form on the rutile $\text{SnO}_2(110)$ surface depending on experimental conditions (e.g. annealing temperatures and oxygen partial pressure) [17, 19]. Often complicated structures with multiple periodicities or multiple structures with identical periodicities are observed [17–19, 21–23]. The complexity of the surface structures has made it difficult to obtain the same level of detailed structural characterisation as for the $\text{TiO}_2(110)$ surface. It is thought that empty Sn states are being sampled in STM studies due to the positive applied bias potential (*i.e.* the bright spots correspond to fivefold-coordinated Sn sites) [23], however there is no detailed study of the contrast in SnO_2 surfaces comparable to to the one for the $\text{TiO}_2(110)$ surface in Ref. [15].

Generally, there are two modes of water adsorption on TiO_2 or SnO_2 surfaces: 1) the molecular adsorption mode and 2) the dissociative adsorption mode. Molecular adsorption involves direct interaction of the oxygen atom of the molecule with the surface fivefold-coordinated metal adsorption site, M_{5c} , forming an adsorbed water molecule, $\text{H}_2\text{O}_{\text{ads}}$. In the dissociative adsorption mode the molecule breaks apart and a hydrogen atom is transferred to a nearby oxygen atom. Two surface hydroxyls are formed: the hydroxyl bonded to the surface M_{5c} is generally called the terminal hydroxyl, OH_{TH} ; the one formed from the detached hydrogen and nearby oxygen atom is called the bridging hydroxyl, OH_{BH} . Molecularly and dissociatively adsorbed water molecules can therefore result in three immediate adsorbed species: $\text{H}_2\text{O}_{\text{ads}}$, OH_{TH} and OH_{BH} .

There is an extensive body of research reporting investigations on the adsorption of water on the defect-free rutile $\text{TiO}_2(110)$ surface. The long-standing debate about whether water molecules are adsorbed molecularly or dissociatively on this surface has been the subject of many of these studies. A brief summary of this work is provided in Sec. II, although for a more complete review, refer to [24] and references within.

The purpose of this study is to focus on the first layer of water on the rutile $\text{SnO}_2(110)$ and $\text{TiO}_2(110)$ surfaces in order to understand better the water-water and water-surface interactions. It should be noted that the aim of this study is not to identify which adsorption mode – molecular, dissociative, or mixed – is most energetically stable, but to explore the properties of the surfaces, improve current understanding of the interactions mentioned above, which in turn govern the structure of water on the surface. We have adopted the hybrid-exchange B3LYP functional as it has been shown to reproduce the observed bond distances and energies of intermolecular interactions better than the GGA, in adsorbate-substrate systems of this kind [25]. Furthermore a key advantage provided by the B3LYP functional is its accurate band gap description; this is an important requirement when studying the electronic structure of the system [26, 27]. The results and discussion lead to the idea that water adsorption on rutile $\text{SnO}_2(110)$ could be described by a simple model, whereas on the corresponding TiO_2 surface, a more complex picture arises.

This paper is organised as follows. A brief review of experimental and theoretical studies of water adsorption on the rutile (110) surfaces of SnO_2 and TiO_2 is presented in Sec. II. Sec. III contains the computational details. Results of DFT calculations are presented in Sec. IV. The discussion begins with the optimised geometries of bulk SnO_2 and TiO_2 , followed by the (110) surface formation in both materials. This is followed by an analysis of water adsorbed on the surface by the dissociative adsorption mode at coverages between one monolayer (1 ML) to the effectively isolated case (1/7 ML) on both SnO_2 and TiO_2 (110) surfaces. Then monolayer water adsorption on each surface is discussed. The electronic structure of dissociative and mixed molecular and dissociative adsorption modes is then presented. By analysing the projected density of states of the adsorbate-substrate systems, reasons why adsorbed water has been reported to be unstable on rutile $\text{SnO}_2(110)$ are explored. Computed STM images of the clean surfaces are then presented. Lastly, Sec. V contains the conclusions drawn from this study.

II. BRIEF REVIEW OF PREVIOUS LITERATURE

Surface X-ray diffraction, crystal truncation rod (CTR) measurements, ultraviolet photoelectron spectroscopy (UPS), temperature-programmed desorption (TPD), work function measurements, X-ray photoelectron spectroscopy (XPS), high resolution electron energy loss spectroscopy (HREELS), and photoemission measurements have all contributed to the discussion. Until 1998, the majority of experimental measurements supported the idea that molecular adsorption dominates in the first layer of water ($\Theta \leq 1$ ML) on nearly-perfect surfaces at low temperatures (< 350 K) [28], and that water dissociates only at oxygen vacancy sites [29–39]. An alternative picture of water adsorption on this surface was developed in 1998 using first-principles molecular dynamics simulations [40]. In the calculated hydrogen vibrational power spectrum, both water bond-bending $\delta(\text{HOH})$ and O-H stretching $\nu(\text{OH})$ signals were observed. This work proposed the coexistence of molecularly adsorbed and dissociatively adsorbed water on the defect-free rutile $\text{TiO}_2(110)$ surface at monolayer coverage ($\Theta = 1$ ML), where this mixed adsorption mode was stabilised by intermolecular hydrogen bonding interactions between the $\text{H}_2\text{O}_{\text{ads}}$ and OH_{TH} adsorbed species. Interestingly in a more recent experimental study, Walle *et al.* presented evidence of both molecularly and dissociatively adsorbed water using photoemission measurements under UHV conditions and at low temperature, on a relatively defect-free surface [41]. Many of the early theoretical studies indicate that the dissociative adsorption mode is energetically favoured on the defect-free $\text{TiO}_2(110)$ surface at all coverages up to 1 ML [42–52]. Many of these simulations are, however, based on models imposing either point group or translational symmetry constraints. In calculations of this type, translational symmetry constraints must be removed in order to study intermolecular interactions reliably even at monolayer coverage [40]. A number of theoretical studies have consequently emphasised the need to study intermolecular interactions [40, 52–54]. Collectively, this research has led to a fairly consistent picture of the behaviour of water on the near ideal rutile $\text{TiO}_2(110)$ surface. Isolated molecules tend to be adsorbed dissociatively, and at higher coverages molecular adsorption is possible when stabilised by hydrogen bonding to an adjacent adsorbate.

In contrast to the large number of articles in the literature on water adsorption on rutile $\text{TiO}_2(110)$, experimental and theoretical water adsorption studies on rutile $\text{SnO}_2(110)$ are less extensive. One of the research questions that has been addressed by a number

of studies in this field is whether molecular adsorption is stable on the rutile $\text{SnO}_2(110)$ surface, and the extent of dissociation. Comparison to $\text{TiO}_2(110)$ provides insight into the effect of small changes in the structure of the surface on the adsorption of water and the interactions involved. An early experimental study by Gercher and Cox [55] sparked the discussion in 1995; temperature-programmed desorption (TPD) and ultraviolet photoelectron spectroscopy (UPS) measurements indicated that molecular adsorption can be stable on the rutile $\text{SnO}_2(110)$ surface. In this study, it was concluded that the amount of dissociation was 10-15% on reduced and highly-defective surfaces. This percentage increased to 35% on less defective surfaces [55]. One of the earliest theoretical studies to follow this experimental evidence was presented by Goniakowski and Gillan; in this paper, the authors studied the molecular and dissociative adsorption modes of water on both $\text{SnO}_2(110)$ and $\text{TiO}_2(110)$ surfaces by using plane-wave pseudopotential density functional theory (DFT) calculations with the Becke-Perdew (BP) scheme within the Generalised Gradient Approximation (GGA) [47]. They reported that both adsorption modes on each material were energetically favourable, in agreement with the experimental evidence. However, it was pointed out by Lindan [56] that these calculations did not address intermolecular interactions, a vital component when studying water adsorption at oxide surfaces. Further GGA calculations by Lindan using the Perdew-Wang (PW) functional suggested that hydrogen bonding is less advantageous on $\text{SnO}_2(110)$ than $\text{TiO}_2(110)$ because of its larger lattice parameters, *i.e.* due to geometrical differences. It was noted however that there must be other factors involved [56]. Bates predicted, using the same methodology, that at monolayer coverage, 50% or more of molecules dissociate on the perfect rutile $\text{SnO}_2(110)$ surface [57], and that molecular water is stable in the mixed adsorption mode (which contains both molecularly and dissociatively adsorbed water). In this study, chains of molecularly adsorbed water molecules along the \mathbf{a}_{slab} direction ([001] direction of the bulk) were found to dissociate. More recently, theoretical studies have found stable molecular adsorption configurations along \mathbf{a}_{slab} . Evarestov *et al.* presented DFT calculations based on the linear combination of atomic orbitals (LCAO) using the hybrid-exchange B3LYP functional, that in contrast to former plane-wave GGA calculations evaluated stable molecular adsorption on this surface [25]. They suggested that this is because the functional B3LYP provides a more accurate description of the energy and bond distances for hydrogen-bonded systems than when using local or semi-local DFT functionals. Bandura *et al.* then investigated the adsorption of water on $\text{SnO}_2(110)$ compared

with $\text{TiO}_2(110)$ using the Perdew, Burke and Ernzerhof (PBE) GGA functional [58]. Their computed energies were in agreement with earlier plane-wave GGA studies in that adsorbed water molecules are stable on $\text{SnO}_2(110)$ if they are neighboured by dissociated molecules, *i.e.* in the mixed adsorption mode, whereas in the case of $\text{TiO}_2(110)$, all three adsorption modes – molecular, dissociative, and mixed – were found to be stable in the calculations. In this paper, the authors suggested an alternative model for describing the relative stability of molecularly adsorbed water on $\text{SnO}_2(110)$: the basicity of the bridging oxygen ion on $\text{SnO}_2(110)$ is greater than that on $\text{TiO}_2(110)$ and so the water molecule interacting with $\text{SnO}_2(110)$ involves a larger redistribution of water states. The most recent work on water adsorption on $\text{SnO}_2(110)$ and comparison with $\text{TiO}_2(110)$ also adopted GGA with the PBE functional and found a stable configuration of purely molecular adsorption at monolayer coverage on $\text{SnO}_2(110)$, made possible by using a large simulation cell to reduce the level of symmetry imposed on the system [59]. The dissociative adsorption mode was still more favourable at all coverages. On $\text{TiO}_2(110)$, isolated water molecules tended to dissociate and molecularly adsorbed water at monolayer coverage was found to be the most favourable adsorption mode. It is clear that adsorption energetics are sensitive to electronic structure methods and differences in computational models. Small energetic differences between binding energies of different adsorption modes also suggests the coexistence of molecularly and dissociatively adsorbed water at monolayer coverage on the rutile $\text{SnO}_2(110)$ surface at standard room temperature and pressure.

III. COMPUTATIONAL DETAILS

All calculations have been performed using the CRYSTAL09 software package [60, 61], based on the expansion of crystalline orbitals as a linear combination of a local basis set (BS) consisting of atom-centred Gaussian orbitals. The titanium, tin and oxygen atoms are described by a triple valence all-electron BS: an 86-411G** contraction (one s , four sp and two d shells), a 976-311G*** contraction (one s , five sp and three d shells), and an 8-411G* contraction (one s , three sp and one d shells), respectively [62, 63]. These basis sets were developed in previous studies of the bulk and surface phases, in which a systematic hierarchy of all-electron basis sets was used to quantify the effects of using a finite BS [64, 65]. The hydrogen atom is described by two s and one p shells, corresponding to a

6-31G** contraction [66]. The DFT method invokes the Born-Oppenheimer approximation in which the nuclei are assumed to be fixed in position relative to the electrons. The impact of including quantum nuclear effects on the hydrogen bonds in water is modest: the differences in hydrogen bonds can be attributed to inaccuracies in the PES, contributing 0.002-0.004eV per H bond, and to inaccuracies in the estimation of the zero-point energies, which contributes 0.015-0.018eV per H bond [67]. In the light of the water-oxide systems in the current work, the contribution of these effects to the BE differences in molecular, dissociative and mixed adsorption modes would be very much smaller and thus negligible. Furthermore, the quality of the oxygen and the hydrogen BS in describing the water molecule has been assessed in previous work [24].

Electronic exchange and correlation are approximated using the hybrid-exchange B3LYP functional. Matrix elements of the exchange and correlation potentials and the energy functional are integrated numerically on an atom-centred grid of points. The integration over radial and angular coordinates is performed using Gauss-Legendre and Lebedev schemes, respectively. A pruned grid consisting of 99 radial points and 5 sub-intervals with (146, 302, 590, 1454, 590) angular points has been used for all calculations (the XXLGRID option implemented in CRYSTAL09 [60]). This grid converges the integrated charge density to an accuracy of about $\times 10^{-6}$ electrons per formula unit. The Coulomb and exchange series are summed directly and truncated using an overlap criterion with thresholds of 10^{-7} , 10^{-7} , 10^{-7} , 10^{-7} and 10^{-14} as described previously [60, 68]. Reciprocal space sampling for the bulk structure was performed on a Pack-Monkhorst net with a shrinking factor of 8 along each periodic direction, generating 75 \mathbf{k} -points in the irreducible Brillouin zone (IBZ).

With regards to the surface [61], slabs consisting of 9-atomic-layers (9AL) and 18AL have been adopted to investigate water adsorption on $\text{SnO}_2(110)$ since the surface formation energy converges with respect to slab thickness to within 0.02 Jm^{-2} at 18AL (see Sec. IV B). The study of monolayer water adsorption in Sec. IV C 2 also contains results for the 21AL slab. The $\text{TiO}_2(110)$ surface formation energy has been reported to oscillate significantly, so 9AL, 18AL, 21AL, 33AL and 36AL slabs were used to model water chemistry in this study. The shrinking factors [8,8], [4,8], [4,8], [2,8], [2,8], [2,8] and [2,8] were adopted along the two periodic directions for 1x1, 2x1, 3x1, 4x1, 5x1, 6x1 and 7x1 surface unit cells, respectively, in order to ensure consistent \mathbf{k} -space sampling. The self-consistent field procedure was converged up to a tolerance in the total energy of $\Delta E = 1 \cdot 10^{-7} E_h$ per unit cell.

Structural optimisation was performed using the Broyden-Fletcher-Goldfarb-Shanno scheme, as implemented in CRYSTAL09 [60]. Convergence was determined from the root-mean-square (rms) and the absolute value of the largest component of the forces. The thresholds for the maximum and the rms forces (the maximum and the rms atomic displacements) have been set to 0.00045 and 0.00030 (0.00180 and 0.0012) in atomic units. Geometry optimisation was terminated when all four conditions were satisfied simultaneously.

For the water adsorption energetics, the binding energy (BE) per molecule of the adsorbate-substrate system was computed with respect to the isolated molecule and the clean surface. The counterpoise correction to the binding energy was applied to take into account the basis set superposition error (BSSE), details of which are documented in Ref. [69, 70]. In addition, it should be noted that molecules were adsorbed symmetrically on each side of the slab. The electronic structure of the adsorbate-substrate system was studied by carrying out projection of density of states following a Mulliken analysis.

For the simulation of constant current STM images, diffuse orbitals were added to the basis sets of all under-coordinated Ti and O ions for the $\text{TiO}_2(110)$ surface. For the Ti (O) ions an extra d (p) orbital was added with $\alpha = 0.06 \text{ bohr}^{-2}$. The resulting (enhanced) basis sets are described in detail in Ref. [71]. This methodology has been shown to accurately reproduce STM images for low-index surfaces of anatase and rutile TiO_2 [71]. To reflect the positive bias used experimentally [15], the states sampled in this study were those within 1 eV of the conduction band minimum. The 1 eV reflects a typical applied bias for STM images of this surface [15]. For the $\text{SnO}_2(110)$ surface, diffuse orbitals were added to the basis sets of all under-coordinated Sn and O atoms. An extra sp orbital was added to the basis sets of the Sn and O ions with $\alpha = 0.06 \text{ bohr}^{-2}$. As with TiO_2 , the states sampled were within 1 eV of the conduction band minimum, reflecting typical applied bias potentials [17, 23].

IV. RESULTS AND DISCUSSION

The bulk structures of rutile SnO_2 and TiO_2 are presented in Sec. IV A as a reference; the (110) surface formation in both materials is discussed in Sec. IV B. The dissociative adsorption mode at low coverage ($\Theta = 1/7 \text{ ML}$) up to monolayer coverage ($\Theta = 1 \text{ ML}$) on both SnO_2 and TiO_2 (110) surfaces is compared in Sec. IV C 1. Following this, in Sec. IV C 2 monolayer adsorption on each surface is analysed in terms of binding energies and hydrogen

bond lengths between adjacent adsorbates. The electronic structure of monolayer water in contact with the $\text{SnO}_2(110)$ and $\text{TiO}_2(110)$ surfaces is discussed in Sec. IV D, and lastly, STM simulations of the clean surfaces are presented in Section IV E.

A. Bulk Rutile SnO_2 and TiO_2

SnO_2 and TiO_2 are isostructural, both being characterised by sixfold-coordinated metal ions and threefold-coordinated oxygen ions, which form SnO_6 and TiO_6 octahedra, as shown in Fig. 1. The values of the internal coordinate u of each material are also very similar, which can be seen in Table I. The structural difference between SnO_2 and TiO_2 lies in the unit cell dimensions. The calculated \mathbf{a} and \mathbf{c} lattice parameters of SnO_2 and TiO_2 agree well with those measured using X-ray diffraction at 298 K with small percentage deviations between 0.68% and 2.13%, as shown in Table I. The values of \mathbf{a} and \mathbf{c} for SnO_2 are 0.183 Å and 0.275 Å larger than those of TiO_2 , respectively. The effect of the enlarged lattice parameters of SnO_2 on intermolecular interactions between adsorbates will be discussed in Sec. IV C. From an electronic point of view, Sn^{4+} and Ti^{4+} ions both have complete shells, with atomic configurations of $[\text{Kr}]4d^{10}$ and $[\text{Ne}]3s^2 3p^6$, respectively. In terms of size, sixfold-coordinated Sn^{4+} and Ti^{4+} ions have ionic radii of 0.605 Å and 0.690 Å, respectively; so Sn^{4+} is the larger ion of the two [72].

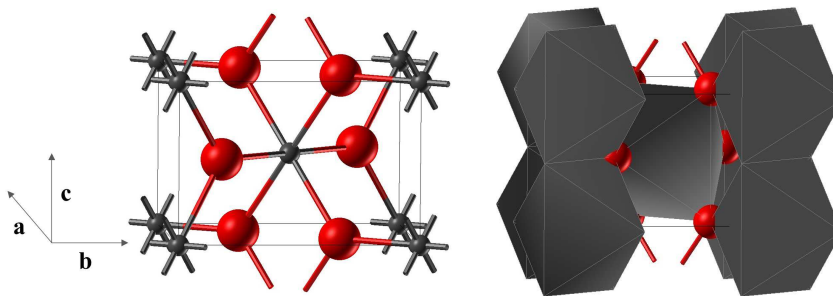


FIG. 1. The structure of the unit cell (left) and the metal-oxygen MO_6 octahedra (right), characterising bulk rutile SnO_2 and TiO_2 . Lattice parameters \mathbf{a} , \mathbf{b} , and \mathbf{c} correspond to the [100], [010] and [001] directions, respectively. The metal (M) and oxygen (O) ions are represented by grey and red spheres and the unit cell is represented by a grey line. If viewed in black and white: M and O ions appear as dark grey and light grey spheres, respectively.

TABLE I. Calculated and experimental values of lattice parameters \mathbf{a} and \mathbf{c} , and the internal coordinate u of bulk rutile SnO_2 and TiO_2 . The calculations have been carried out using the DFT hybrid-exchange B3LYP functional. Experimental values (X-ray diffraction at 298 K) are from the given references [73, 74]. The percentage deviation of the calculated values from experiment are shown in parentheses.

	$\mathbf{a} = \mathbf{b}$ (Å)		\mathbf{c} (Å)		u		Ref.
	Opt.	Exp.	Opt.	Exp.	Opt.	Exp.	
SnO_2	4.822 (1.79%)	4.737	3.254 (2.13%)	3.186	0.307 (0.00%)	0.307	[73]
TiO_2	4.639 (0.98%)	4.594	2.979 (0.68%)	2.959	0.306 (0.33%)	0.305	[74]

B. The (110) Surfaces of Rutile SnO_2 and TiO_2

The (110) surface for the study of water chemistry is modelled by using a slab cut from the optimised bulk structure along the (110) plane. The structure of the rutile $\text{SnO}_2(110)$ and $\text{TiO}_2(110)$ surfaces, characterised by fivefold-coordinated metal (Sn_{5c} and Ti_{5c}) and twofold-coordinated “bridging” oxygen ions (O_{2c}), is illustrated in Fig. 2, and the corresponding surface unit cell parameters are given in Table II. The \mathbf{a}_{slab} and \mathbf{b}_{slab} parameters of $\text{SnO}_2(110)$ are 0.275 Å (9.23 %) and 0.259 Å (3.95 %) larger than those of $\text{TiO}_2(110)$, respectively. Although the surfaces are very similar in structure, the difference in the lattice parameters of the surface unit cells affects the behaviour of water on this surface facet.

TABLE II. Calculated values of the (110) surface unit cell parameters \mathbf{a}_{slab} and \mathbf{b}_{slab} , corresponding to the [001] and $[1\bar{1}0]$ directions of the bulk, respectively, for rutile SnO_2 and TiO_2 . The $\text{SnO}_2(110)$ \mathbf{a}_{slab} and \mathbf{b}_{slab} parameters are larger than those of $\text{TiO}_2(110)$ by the percentage shown in brackets.

	\mathbf{a}_{slab} (Å)	\mathbf{b}_{slab} (Å)
SnO_2	3.254 (9.23 %)	6.820 (3.95 %)
TiO_2	2.979	6.561

The surface formation energies (E_s) of the two surfaces have been converged with respect to the number of atomic layers (AL). In the case of $\text{SnO}_2(110)$, there is some oscillation between the E_s values of slabs with odd and even number of atomic layers, but it converges with respect to slab thickness at 18AL to within 0.02 Jm^{-2} , with an E_s value of 1.36 Jm^{-2}

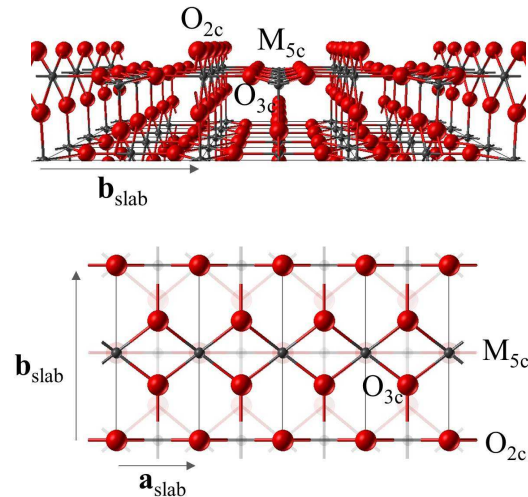


FIG. 2. The structure of the (110) surfaces of rutile SnO_2 and TiO_2 is shown in perspective (top) and from a top view (bottom). The \mathbf{a}_{slab} and \mathbf{b}_{slab} vectors are indicated, corresponding to the [001] and $[1\bar{1}0]$ directions of the bulk, respectively. The surface fivefold-coordinated metal (M_{5c}), twofold-coordinated bridging oxygen (O_{2c}), as well as the surface threefold-coordinated oxygen (O_{3c}) ions are opaque, whereas the lower layers of the slab are translucent. M and O ions are represented by grey and red spheres, respectively. The surface unit cell is represented by a black line. If viewed in black and white: M and O ions appear as dark grey and light grey spheres, respectively.

(see Fig. 3). In the current study, 9AL, 18AL and 21AL slabs have been used to model water adsorption on $\text{SnO}_2(110)$, the results of which are presented in Sec. IV C to Sec. IV D. $\text{TiO}_2(110)$ displays a large oscillation, with odd and even slabs having different E_s values: 0.36 Jm^{-2} and 0.26 Jm^{-2} at 33AL and 36AL, respectively. This oscillation has been given a number of explanations in the literature. The effect has been explained by surface-induced hybridization of Ti-3d and O-2p orbitals among the layers [75], surface dipoles induced by surface relaxations [76], and surface lattice dynamics mediating a long-range electrostatic interaction [77]. Our focus in this work is on the water-water and water-surface interactions in the first layer of water on the (110) surfaces. To allow direct comparison of water energetics to those for $\text{SnO}_2(110)$, 9AL, 18AL and 21AL $\text{TiO}_2(110)$ slabs were used. When discussing water adsorption at monolayer coverage in Sec. IV C 2, 33AL and 36AL $\text{TiO}_2(110)$ slabs have also been included.

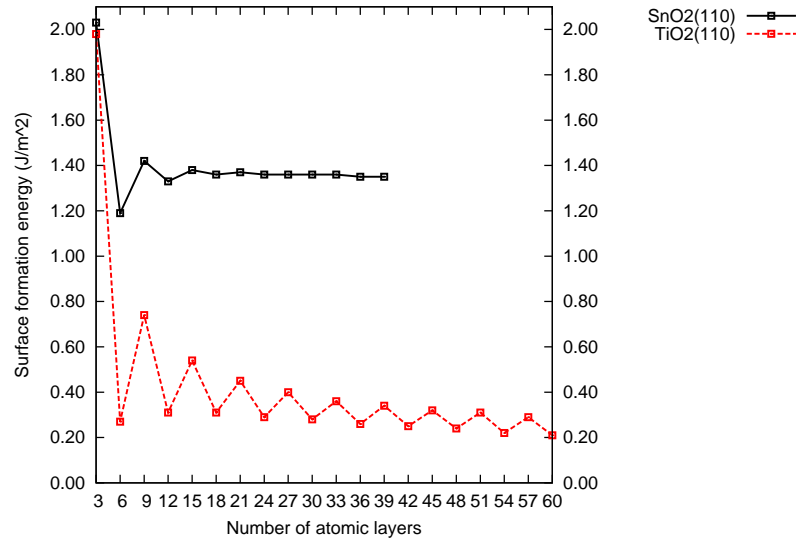


FIG. 3. Surface formation energies (E_s) of rutile SnO_2 and TiO_2 (110) surfaces. The E_s of $\text{SnO}_2(110)$ converges at 18AL to 1.36 Jm^{-2} ; the E_s of $\text{TiO}_2(110)$ oscillates significantly with number of atomic layers (AL), converging to different values for odd and even slabs: 0.36 Jm^{-2} and 0.26 Jm^{-2} at 33AL and 36AL, respectively.

C. Water Adsorption Energetics

1. The Dissociative Adsorption Mode at Low Coverage: $\Theta = 1/7 \text{ ML}$ to 1 ML

In this section, the dissociative water adsorption mode on rutile $\text{SnO}_2(110)$ and $\text{TiO}_2(110)$ is studied in detail. Water was adsorbed dissociatively at coverages between one monolayer ($\Theta = 1 \text{ ML}$) to the effectively isolated case ($\Theta = 1/7 \text{ ML}$). To study the intermolecular interactions between adsorbed hydroxyls, which are strongest in the \mathbf{a}_{slab} direction as demonstrated in previous work [24], the binding energy (BE) per molecule was calculated as a function of coverage and separation of adsorbates in \mathbf{a}_{slab} . Supercells of 1×1 to 7×1 were used to increase the separation from 3.254 \AA to 22.778 \AA and decrease the coverage from $\Theta = 1 \text{ ML}$ to $1/7 \text{ ML}$, as shown in Fig. 4. The reason why a similar study for molecular adsorption has not been included is because adsorbed water molecules on the rutile $\text{SnO}_2(110)$ surface dissociated during structural optimisation, which is in agreement with a number of studies that conclude that molecularly adsorbed water on this surface is unstable. Firstly,

the energetics of the 9-atomic-layer (9AL) adsorbate-substrate system are discussed. The binding energies of the 18AL system are then presented. This approach allows us to disentangle the factors contributing to the binding energy step-by-step, in particular the lateral interactions from the interactions mediated by the surface.

On the 9AL SnO₂(110) slab, the binding energy for the dissociative adsorption mode as a function of adsorbate separation adopts a clear relationship, as seen in Table III. The binding energy becomes more negative, corresponding to more favourable adsorption, as coverage decreases from 1 ML to 1/7 ML and the separation between hydroxyls in \mathbf{a}_{slab} increases from 3.254 Å to 13.016 Å (1x1 to 4x1 cells). This suggests that the effective repulsive interactions between hydroxyls are lowered as the separation in the \mathbf{a}_{slab} direction is increased [78]. Progressively the change in the binding energy with separation, ΔBE , decays to zero and once the hydroxyls are separated by this distance, the binding energy becomes constant and the interactions between hydroxyls diminish to zero at approximately 13.02 Å separation on the 9AL SnO₂(110) slab.

It is interesting to note that this trend is less clear in the dissociative adsorption mode on TiO₂(110). The adsorption becomes more favourable as the separation between hydroxyls in \mathbf{a}_{slab} increases from 3.254 Å to 22.778 Å (1x1 to 7x1 cells). The ΔBE decreases until 13.016 Å, after which it fluctuates in value. The more significant change in ΔBE compared with SnO₂(110) can be observed in the plot in Fig. 5 and at the smaller separations could be explained by stronger repulsive interactions between hydroxyls. The fluctuation of ΔBE as well as the observation that the BE continues to decrease at approximately 22.78 Å and the hydroxyl groups are interacting over a much longer distance than when adsorbed onto SnO₂(110) indicates that that as well as repulsion and hydrogen bonding, the distortion in the surface induced by adsorbing hydroxyls and water molecules is an important effect. As introduced in Ref.[24], water chemistry on TiO₂ involves a balance between direct intermolecular interactions and interactions that are mediated through atomic displacements in the surface.

The results of the dissociative adsorption mode on the 18AL (110) slabs of SnO₂ and TiO₂ are in agreement with those for 9AL slabs, except that instead of diminishing completely, the interactions on SnO₂ are reduced significantly at separations above 13.016 Å. From the BE in Table III alongside the plot in Fig. 5, it can be seen that the BE in 9AL and 18AL SnO₂ are similar in value. The 18AL TiO₂ BEs are approximately 1.00-1.20 eV higher in

TABLE III. The binding energy per molecule (BE) of the adsorbate-substrate system with respect to the clean surface and isolated molecule [70] are shown for relaxed geometries in the dissociative adsorption mode on rutile $\text{SnO}_2(110)$ and $\text{TiO}_2(110)$. Binding energies are shown for a range of systems with increasing separation of adsorbates in the \mathbf{a}_{slab} direction. The change in binding energy with increasing separation is noted as ΔBE .

Cell size	Coverage Θ	Separation (\AA)	SnO_2				TiO_2				
			9AL		18AL		9AL		18AL		
			BE (eV)	ΔBE (eV)	BE (eV)	ΔBE (eV)	BE (eV)	ΔBE (eV)	BE (eV)	ΔBE (eV)	
1x1	1	3.254	-1.69	—	-1.61	—	2.979	-0.82	—	-0.39	—
2x1	1/2	6.508	-1.75	-0.06	-1.61	0.00	5.959	-1.21	-0.39	-0.26	0.13
3x1	1/3	9.762	-1.80	-0.05	-1.73	-0.12	8.938	-1.40	-0.19	-0.42	-0.16
4x1	1/4	13.016	-1.81	-0.01	-1.75	-0.02	11.918	-1.46	-0.06	-0.40	0.02
5x1	1/5	16.270	-1.81	0.00	-1.78	-0.03	14.897	-1.61	-0.15	-0.51	-0.11
6x1	1/6	19.524	—	—	-1.81	-0.03	17.874	-1.66	-0.05	-0.45	0.06
7x1	1/7	22.778	—	—	-1.81	0.00	20.853	-1.73	-0.07	-0.52	-0.07

energy than those of 9AL, suggesting that the water adsorption is more favourable on slabs with an odd number of atomic layers than slabs with an even number of atomic layers.

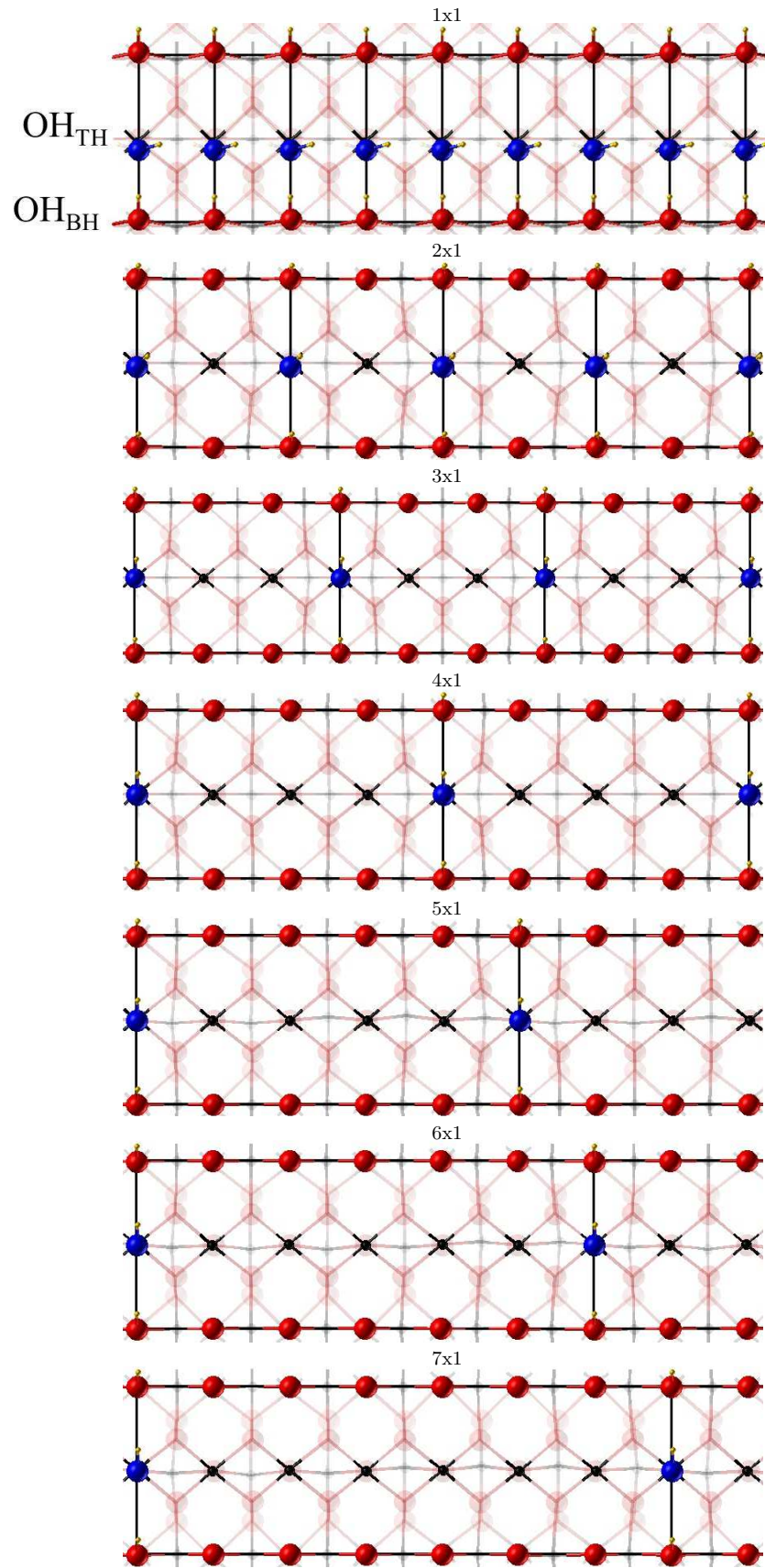


FIG. 4. Top views of the adsorbate-substrate system in the dissociative water adsorption mode on the rutile $\text{TiO}_2(110)$ surface (the rutile $\text{SnO}_2(110)$ surface shares the same structure). The separation between hydroxyls (OH_{TH} and OH_{BH}) in the \mathbf{a}_{slab} direction increases with the size of the surface unit cell from 1×1 to 7×1 . The surface fivefold-coordinated Ti and twofold-coordinated bridging O ions, as well as those atoms belonging to the adsorbate, are opaque, whereas the lower layers of the slab are translucent. Ti, O, adsorbate O, and adsorbate H atoms are represented by black, red, blue, and yellow spheres, respectively. The surface unit cell is represented by a black line. If viewed in black and white: Ti, O and H atoms appear as black, dark grey, and light grey spheres, respectively.

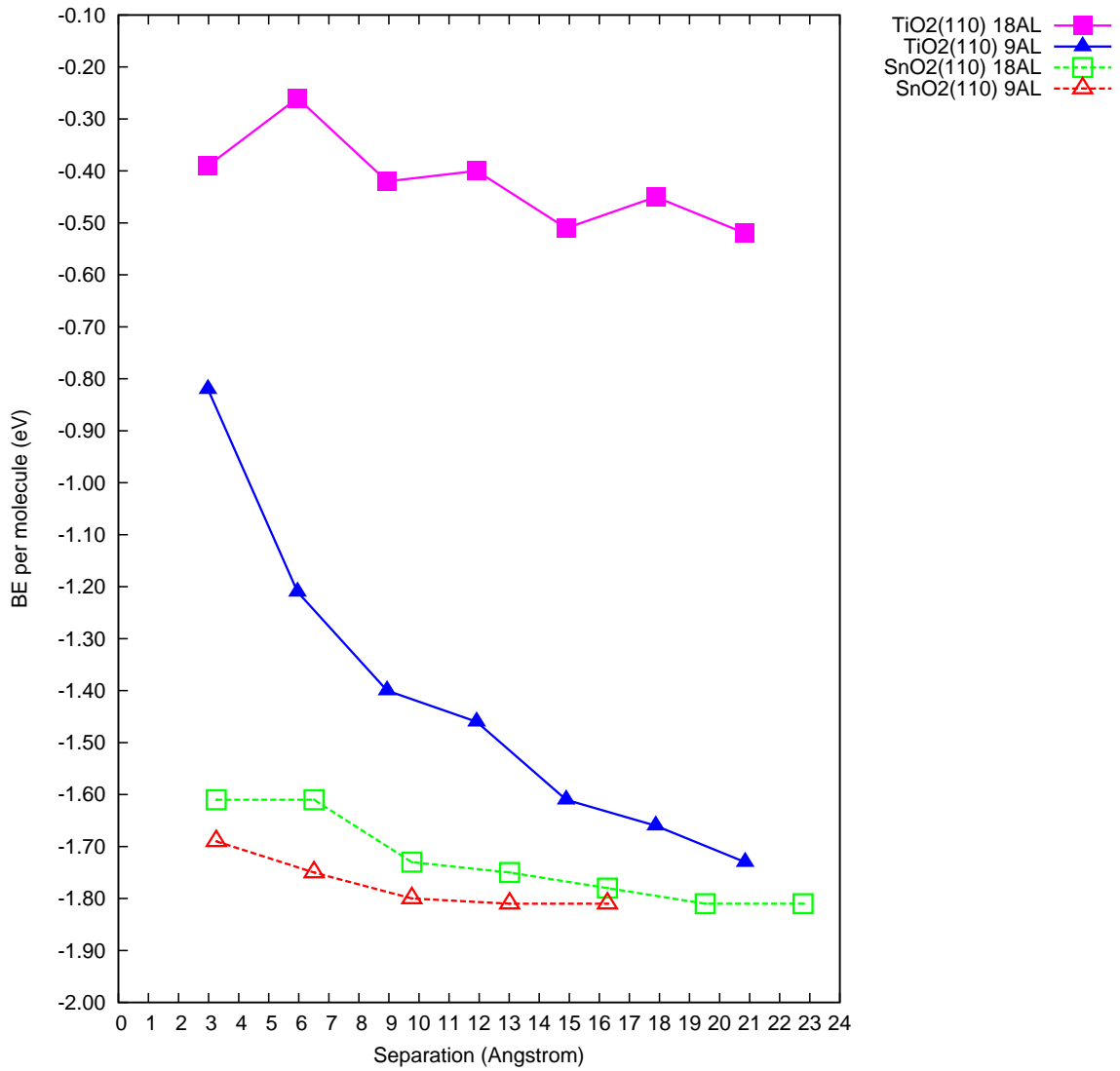


FIG. 5. The binding energy per molecule (BE) as a function of separation of hydroxyls in the \mathbf{a}_{slab} direction for the dissociative adsorption mode. Rutile $\text{SnO}_2(110)$ [$\text{TiO}_2(110)$] slabs are represented by empty triangles (9AL) and squares (18AL) [filled triangles (9AL) and squares (18AL)].

2. Monolayer Adsorption: $\Theta = 1$ ML

In monolayer water adsorption, each fivefold-coordinated metal ion (M_{5c}) site is occupied by an adsorbate, either a terminal hydroxyl (OH_{TH}) or an adsorbed water molecule ($\text{H}_2\text{O}_{\text{ads}}$). Adjacent adsorbates in the \mathbf{a}_{slab} direction on the rutile $\text{TiO}_2(110)$ surface are stabilised by hydrogen bonding [40, 52, 53]. The calculated \mathbf{a}_{slab} parameter of rutile $\text{SnO}_2(110)$ is 0.275 Å (9.23%) larger than that of rutile $\text{TiO}_2(110)$, as discussed in Sec. IV B, and theoretical calculations suggest that it is for this reason that hydrogen bonding is less advantageous on $\text{SnO}_2(110)$ in comparison with $\text{TiO}_2(110)$ [56, 57]. In order to investigate further the intermolecular interactions between adjacent adsorbates on each surface, this section analyses the geometry and energetics of monolayer water adsorption ($\Theta = 1$ ML).

At monolayer coverage, in addition to the dissociative (DD) and molecular (MM) adsorption modes, a mixed dissociative and molecular (DM) adsorption mode can be studied, as shown in Fig. 6. In Table IV, the BE for each mode and the corresponding $\text{SnO}_2(110)$ and $\text{TiO}_2(110)$ slab thicknesses is reported. Both surfaces were modelled using 9AL, 18AL and 21AL slabs, and since the E_s of $\text{TiO}_2(110)$ has been reported to oscillate significantly, both in this study (see Fig. 3) and in the literature [75–77], the adsorption energetics for 33AL and 36AL $\text{TiO}_2(110)$ slabs have also been included here.

The results indicate that molecular adsorption is unstable on the $\text{SnO}_2(110)$ surface, regardless of the slab thickness. Molecules adsorbed in the MM configuration dissociated during the geometry optimisation, resulting in the fully dissociated DD solution. However, adsorbed water molecules are stabilised when adjacent hydroxyls are present in the mixed (DM) adsorption mode with a favourable BE of -1.59 eV on the 18AL slab. This evidence suggests that water molecules can exist on the rutile $\text{SnO}_2(110)$ surface, which is in agreement with experimental observations made by Gercher and Cox [55] (see Sec. I). In terms of slab thickness, the BE converges to within 0.01 eV at 18AL. As shown in Sec. IV B, the surface energy of $\text{SnO}_2(110)$ displays little oscillation and also converges at 18AL. This is consistent with the conventional slab approach to modelling surfaces in which the convergence of the computed properties with the number of layers in the slab is reached and at this point the atoms in the central layers of the slab exhibit bulk-like behaviour.

Interestingly, the BE is more favourable for the dissociative adsorption mode than mixed by 0.02 eV in the converged results. This small BE difference between the two adsorption

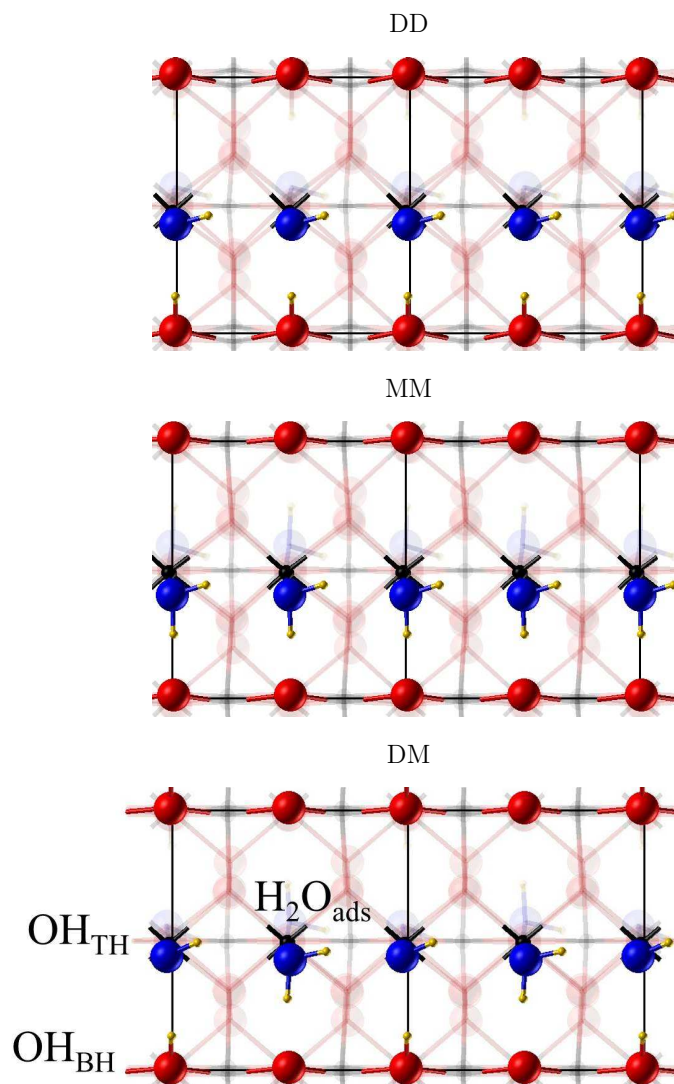


FIG. 6. Top views of the adsorbate-substrate system in monolayer water adsorption ($\Theta = 1$ ML) on the rutile $\text{TiO}_2(110)$ surface, calculated using a 2×1 surface unit cell. The three adsorption modes are shown: dissociative (DD), molecular (MM) and mixed (DM). The surface fivefold-coordinated Ti and bridging O ions, as well as the atoms belonging to the adsorbate, are opaque, whereas the lower layers of the slab are translucent. Ti, O, adsorbate O, and adsorbate H atoms are represented by black, red, blue, and yellow spheres, respectively. The 2×1 surface unit cell is represented by a black line. If viewed in black and white: Ti, O and H atoms appear as black, dark grey, and light grey spheres, respectively.

modes suggests that the intermolecular interactions present between two adjacent termi-

TABLE IV. The binding energy (BE) per molecule for the dissociative, molecular and mixed adsorption modes on the rutile $\text{SnO}_2(110)$ and $\text{TiO}_2(110)$ surfaces of increasing slab thicknesses are shown for monolayer coverage ($\Theta = 1$ ML, 2×1 cell). The number of atomic layers (AL) in the slab for each result is indicated.

Surface		BE / eV		
		Dissociative DD	Molecular MM	Mixed DM
$\text{SnO}_2(110)$	9AL	-1.86	—	-1.68
	18AL	-1.61	—	-1.59
	21AL	-1.62	—	-1.60
$\text{TiO}_2(110)$	9AL	-0.85	-0.99	-1.03
	18AL	-0.39	-0.73	-0.55
	21AL	-0.53	-0.84	-0.74
	33AL	-0.50	-0.82	-0.65
	36AL	-0.39	-0.73	-0.54

nal hydroxyls and between a terminal hydroxyl and adsorbed water molecule are similar in character and strength [79]. Despite the modest energy difference, the stabilisation of the dissociative adsorption mode becomes evident through analysis of the chemisorption and hydrogen bonding interactions. The lengths of the bond generated between the adsorbate oxygen atom (O_{ads}) and the surface fivefold-coordinated metal adsorption site ($\text{M}_{5\text{c}}$), $d(\text{M}_{5\text{c}}\text{O}_{\text{ads}})$, along with the hydrogen bond between adjacent adsorbates, $d(\text{H}_{\text{ads}}\text{O}_{\text{ads}})$, are presented in Table V. The $d(\text{Sn}_{5\text{c}}\text{O}_{\text{ads}})$ in dissociative adsorption is 0.035 - 0.15 Å smaller than the corresponding values in mixed adsorption, indicating stronger chemical bonds in the former. The hydrogen bond $d(\text{H}_{\text{ads}}\text{O}_{\text{ads}})$ in DD between the two adjacent terminal hydroxyls is 2.495 Å whereas in DM, between the terminal hydroxyl and adsorbed water molecule, the length of the interaction increases to 3.253 Å. The stronger chemical and hydrogen bonds observed in the dissociative adsorption mode with respect to mixed adsorption on $\text{SnO}_2(110)$ characterise its favourable BE.

When analysing these results, it is important to take into account the effect of point group and translational symmetry constraints on the optimisation of the system geometry [80]. The calculations presented in this section contain two point group symmetry operators,

TABLE V. Bond lengths in dissociative (DD), molecular (MM) and mixed (DM) adsorption at monolayer coverage ($\Theta = 1$ ML) on rutile $\text{SnO}_2(110)$ and $\text{TiO}_2(110)$ surfaces. $d(\text{M}_{5c}\text{O}_{\text{ads}})$ is the length of the bond between the surface fivefold-coordinated metal adsorption site, M_{5c} , and the oxygen from the adsorbate, O_{ads} . Monolayer adsorption was modelled using two adsorbed water molecules per 2×1 surface cell, therefore the $d(\text{M}_{5c}\text{O}_{\text{ads}})$ value for each adsorbed molecule, either dissociative (D) or molecular (M), is given. In the mixed adsorption case, the first and second values of $d(\text{M}_{5c}\text{O}_{\text{ads}})$ refer to the dissociatively and molecularly adsorbed molecule, respectively. $d(\text{H}_{\text{ads}}\text{O}_{\text{ads}})$ is the hydrogen bond length between the hydrogen of the first adsorbate to the oxygen of the adjacent one.

Surface		Bond length / \AA					
		Dissociative		Molecular		Mixed	
		DD		MM		DM	
		$d(\text{M}_{5c}\text{O}_{\text{ads}})$	$d(\text{H}_{\text{ads}}\text{O}_{\text{ads}})$	$d(\text{M}_{5c}\text{O}_{\text{ads}})$	$d(\text{H}_{\text{ads}}\text{O}_{\text{ads}})$	$d(\text{M}_{5c}\text{O}_{\text{ads}})$	$d(\text{H}_{\text{ads}}\text{O}_{\text{ads}})$
		D, D		M, M		D, M	
$\text{SnO}_2(110)$	9AL	2.054, 2.054	2.495	—	—	2.084, 2.197	3.235
	18AL	2.050, 2.050	2.495	—	—	2.085, 2.200	3.253
	21AL	2.050, 2.050	2.497	—	—	2.085, 2.200	3.253
$\text{TiO}_2(110)$	9AL	1.901, 1.902	2.193	2.254, 2.252	2.171	1.892, 2.306	2.421
	18AL	1.871, 1.870	2.194	2.363, 2.362	2.153	1.931, 2.293	2.520
	21AL	1.883, 1.883	2.194	2.343, 2.341	2.159	1.909, 2.306	2.488
	33AL	1.875, 1.876	2.190	2.361, 2.356	2.153	1.908, 2.310	2.479
	36AL	1.871, 1.871	2.194	2.364, 2.365	2.147	1.911, 2.312	2.481

and the translational symmetry constraints are partially removed. Monolayer coverage can be modelled by the adsorption of one water molecule per 1×1 surface unit cell, where each molecule on the surface is equivalent. In these results, monolayer coverage has been modelled by the adsorption of two inequivalent molecules in a larger 2×1 surface unit cell. Although the atomic configurations in the two cases are equivalent, the latter situation involves the

removal of translational symmetry giving the atoms more freedom to relax. This method is necessary for studying the interactions between two inequivalent adjacent adsorbates at monolayer coverage.

In contrast to $\text{SnO}_2(110)$, all three adsorption modes – dissociative, molecular and mixed – are stable on the $\text{TiO}_2(110)$ surface. Molecular adsorption has more favourable BEs than the dissociative and mixed adsorption modes at all slab thicknesses by 0.31-0.34 and 0.10-0.19 eV, with the exception of the 9AL result (where DM is stable by only 0.04 eV with respect to MM). The mixed adsorption mode has the second most favourable BE out of the three modes. This overall stability of all three adsorption modes suggests that there is likely to be a mixture of species and adsorption configurations in the first layer of water on the $\text{TiO}_2(110)$ surface.

The convergence of the BE with respect to slab thickness is also very different to the $\text{SnO}_2(110)$ system. The adsorbate- TiO_2 systems can be separated into two categories: those consisting of an odd and an even number of atomic layers, oAL and eAL. As with the surface formation energies in Sec. IV B, the differences between the oAL and eAL could be explained by surface-induced hybridization of Ti-3d and O-2p orbitals among the layers [75], differences in surface dipoles [76], as well as surface lattice dynamics mediating a long-range electrostatic interaction [77]. It should be noted that rutile TiO_2 is classified as an incipient ferroelectric material: it is close to a ferroelectric transition with respect to the transverse optic (TO) A_{2u} vibrational mode which has a low frequency at room temperature and remains stable even as the temperature is lowered [81, 82]. The lattice dynamics are very sensitive to the lattice parameters, as reported in an earlier study [83]. In this work it was found that upon expansion of the lattice, the TO A_{2u} vibrational mode becomes soft and it was concluded that bulk rutile TiO_2 is unstable with respect to a distortion along the soft TO A_{2u} vibrational mode [83]. Consequently, it is possible that soft vibrational modes in the bulk could propagate through the eAL and oAL slabs, causing odd-even oscillations in the binding energies. The BEs for the eAL converge within 0.01 eV to -0.39, -0.73 and -0.54 eV in DD, MM and DM modes, respectively. In the case of the oAL systems, the DD and MM modes converge within 0.03 eV to -0.50 and -0.82 eV, respectively; however, there is more fluctuation in the BE for the DM configuration and it does not tend to a single value. A possible explanation for this could be associated with the competition between atoms in the slab to accommodate the distortion induced by the hydroxyls and adsorbed

water molecule in the mixed mode. The fact that this competition for the distortion in the oAL system is detrimental to the BE, whereas in the eAL system this effect is absent, could be attributed to the differences in symmetry in slabs containing an odd or even number of atomic layers. Slabs with odd and even number of atomic layers have different symmetry elements. This leads to different degrees of freedom in the atoms. In the case of oAL, there is a central plane of atoms restricted by its symmetry, whereas in eAL slabs the absence of the centre plane of atoms means that the displacements induced by distortion at each surface of the slab are accommodated in the bonds.

The relevant bond lengths in the adsorbate-TiO₂(110) system, listed in Table V, carry some interesting observations. The $d(\text{Ti}_{5c}\text{O}_{ads})$ lengths in dissociatively and molecularly adsorbed water are quite different, by roughly 0.5 Å, whereas in the SnO₂(110) case this value is approximately 0.1 Å. This indicates that on rutile TiO₂(110), dissociated and intact molecules interact with the surface in very different ways. Despite the weaker chemisorption bond in molecular adsorption, the stabilisation of the MM configuration on TiO₂(110) is evident from its favourable hydrogen bond length ($d(\text{H}_{ads}\text{O}_{ads}) \sim 2.15$ eV). On a final observation, the relative stability of the mixed adsorption mode with respect to the dissociative in terms of BE is not immediately obvious from the chemisorption and hydrogen bond lengths. The $d(\text{Ti}_{5c}\text{O}_{ads})$ lengths in DD are 0.04-0.44 Å smaller in length than in DM, and the $d(\text{H}_{ads}\text{O}_{ads})$ in DD is ~ 0.29 Å smaller in length than that in DM. The evidence suggests that propagation of atomic displacements in the slab, induced by the distortion at the surface upon adsorption, impact the binding energy of adsorbing species.

In summary, it is clear from the hydrogen bond lengths in Table V that in SnO₂(110) the $d(\text{H}_{ads}\text{O}_{ads})$ distance is unfavourable for strong hydrogen bonding between adjacent adsorbates. By analysing closely the geometry and energetics of water adsorption on both SnO₂(110) and TiO₂(110), it seems that the BEs on SnO₂(110) are mainly governed by the strength of the chemisorption and hydrogen bonds at the surface of the adsorbate-substrate system. On TiO₂(110), a more complicated scenario arises, involving an interplay between chemisorption, hydrogen bonding and distortion in the surface induced by adsorbing hydroxyls and water molecules.

D. Electronic Structure

In this section, the projected density of states (PDOS) of the SnO₂(110) and TiO₂(110) surfaces in contact with monolayer water are presented. Aiming to understand how differences in the electronic structure of SnO₂ and TiO₂ adsorbate-substrate systems affect the water chemistry at the surface, the valence band (VB) and conduction band (CB) states of each material are described, with separate projections onto the M_{5c} and O_{2c} ions. The states of the adsorbed hydroxyls and molecularly adsorbed water molecules are identified relative to the surface Sn/Ti and O states, and the interaction between the adsorbates with each surface is discussed.

The PDOS for mixed dissociative and molecular adsorption at monolayer coverage on both SnO₂(110) and TiO₂(110) surfaces are shown in Fig. 7. The projections onto atoms belonging to the surface show the contributions of the CB (\sim -3 eV), upper VB (\sim -12 eV), and lower VB (\sim -25 eV), which are made up largely of Sn-5s/Sn-5p, O-2p and O-2s states in SnO₂(110), respectively, and Ti-3d, O-2p and O-2s states in TiO₂(110) [84].

The contributions of the dissociatively and molecularly adsorbed molecules are displayed within the PDOS plots. In both materials, the states at \sim -28.5 eV and \sim -15.2 eV characterise the intact water molecules on the surface. It is interesting to note that in TiO₂(110), these peaks, made up largely of O-2p and O-2s states, display significant hybridisation with the O states of the surface. A small amount of hybridisation of the corresponding adsorbed water molecule peaks on SnO₂(110) with the surface VB states can be seen. The lesser interaction of water molecules on SnO₂(110) compared with TiO₂(110) is in agreement with the adsorption energetics and geometry monolayer coverage presented in Sec. IV C 2, in that the molecular adsorption mode MM is unstable on SnO₂(110). The bridging hydroxyls (BH) contribute mainly to the states at \sim -27.0 eV and \sim -14.5 eV on TiO₂(110) and at \sim -27.5 eV on SnO₂(110). Slightly higher in energy than the BH peaks are the terminal hydroxyl (TH) states at \sim -26.5 eV and \sim -14.0 eV on TiO₂(110) and at \sim -26.8 eV and \sim -15 to \sim -9 eV on SnO₂(110). The relative energies of the adsorbate states are in agreement with a previous study by Bandura *et al.* that used the PBE-GGA functional to compare the density of states of mixed adsorption on the two surfaces [58]. In contrast with the adsorbed water molecule states, the states characterising the BH and TH on SnO₂(110) hybridise strongly with the upper and lower VB, which could be related to the stability of the dissociative adsorption

mode on this surface and explain why the DD configuration in Sec. IV C 2 is more favourable than DM. Interestingly, all adsorbate states on $\text{TiO}_2(110)$ display strong hybridisation with its surface VB. In $\text{TiO}_2(110)$, O-2*p* states associated with both the BH and TH are present at the valence band maximum (VBM), whereas those of the adsorbed water molecule appear further from the VBM. This effect is seen also on $\text{SnO}_2(110)$, and becomes important when considering the interaction of charges with adsorbed species.

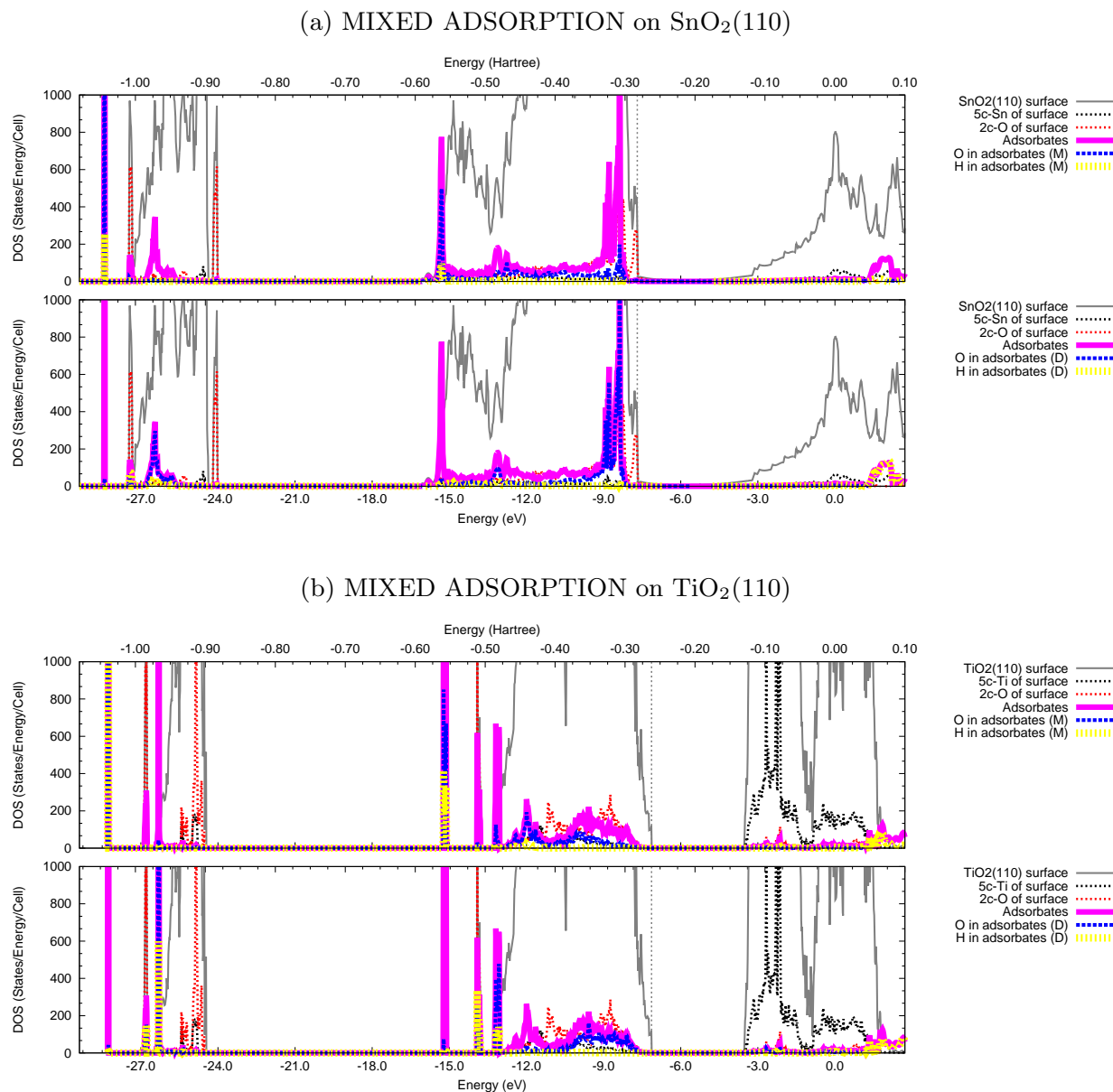


FIG. 7. Projected density of states (PDOS) for the mixed adsorption of water onto (a) the rutile SnO₂(110) surface and (b) the rutile TiO₂(110) surface ($\Theta = 1$ ML; 2×1 cell; 21Å slab). The DOS is projected onto the M_{5c} and O_{2c} of the surface and the O and H atoms in the molecularly (top) and dissociatively (bottom) adsorbed water molecules on each surface. The vertical dotted line in the DOS denotes the position of the Fermi energy. All energies are referred to vacuum zero as 2D periodic boundary conditions are used: $V(z)=0$ when $z \rightarrow \infty$, where V is the electrostatic potential and z is the distance from the surface.

E. STM Simulation

In this section simulated STM images of the SnO_2 and $\text{TiO}_2(110)$ surfaces are presented and compared to each other as well as to the literature. It has been demonstrated that using an atom-centered Gaussian basis set optimised for the ground state energy does not describe the long range tails of the valence and conduction bands in the vacuum above the surface sufficiently accurately [71, 85]. Two modifications have been proposed to obtain constant current STM images in good agreement with experimental images from this type of calculation for rutile TiO_2 surfaces. One involves the addition of empty functions above the surface [85], whilst the other involves the addition of more diffuse functions to the basis sets of surface atoms [71]. For the STM images produced here we have chosen the latter approach, due to its relative simplicity.

In accordance to Ref. [71], additional d and p functions were added to the basis sets of the undercoordinated Ti and O at the rutile $\text{TiO}_2(110)$ surface. This is due to the prominence of Ti-3*d* states (and some hybridisation from O-2*p* states) near the bottom of the CB. The resulting STM image is shown in Fig. 8. The bright spots are above the fivefold-coordinated Ti ions and the area above the undercoordinated O ions is dark, in good agreement with the literature [15, 71, 85].

The choice of functions to be added to the SnO_2 basis sets was not as simple. The bottom of the conduction band is dominated by Sn-5*s* orbitals, but there are significant contributions from Sn-5*p*, O-2*s* and O-2*p* orbitals. Applying the same logic as for the TiO_2 , diffuse p and s orbitals were added to both Sn and O ions. The resulting STM image is shown in Fig. 8. The brightest spots are centered on Sn ions, as predicted in the literature [23]. However, we note here that there are some less bright spots above the bridging O ions as well. Although these are significantly less bright than the ones attributed to the fivefold-coordinated Sn, their presence could be significant. We propose that small changes in bias potential and/or current could lead to the imaging of the O ions instead.

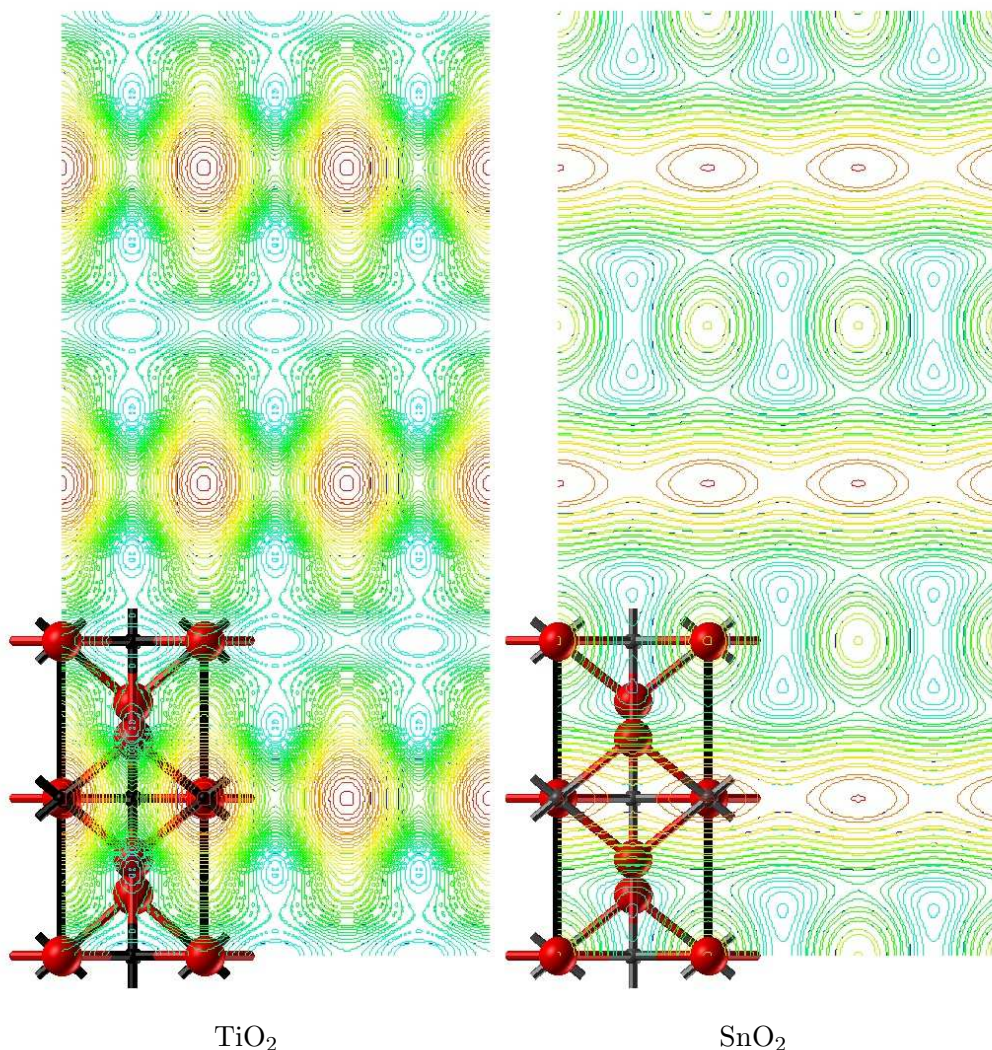


FIG. 8. Simulated constant current STM images for TiO₂ and SnO₂ rutile (110) surfaces. These are contour maps of the charge density isosurface at 5×10^{-6} electrons/bohr³ and 1V sample bias. For the TiO₂ additional diffuse *p* and *d* functions were added to the surface O and Ti basis sets, respectively. For the SnO₂ additional diffuse *s* and *p* functions were added to both the surface O and surface Sn basis sets. In these images the largest values of height (red contours), comparable to bright spots on STM images, are located above the Ti and Sn ions.

V. CONCLUSIONS

In this study, the first layer of water at model oxide surfaces has been explored by comparing the structure and properties of SnO₂(110) and TiO₂(110) surfaces in contact with water. The interesting effects of the structural and electronic differences in the two

materials on the water chemistry deepen the current understanding of water-water and water-surface interactions and could facilitate the prediction of the structure and properties of other oxide-water interfaces.

The dissociative adsorption mode at low coverage (1/7 ML) up to monolayer coverage (1 ML) on both SnO₂ and TiO₂(110) surfaces was analysed. On SnO₂(110), the adsorption becomes more favourable as coverage decreases from 1 ML to 1/7 ML and the separation between hydroxyls in the \mathbf{a}_{slab} direction increases from 3.254 Å to 13.016 Å after which the interactions are reduced significantly. This indicates that the effective repulsive interactions between hydroxyls are lowered as the separation in the \mathbf{a}_{slab} direction is increased. On TiO₂(110), a strong interaction between hydroxyls remains at 22.78 Å separation. As a function of this separation, the BEs fluctuate in value, which suggests that as well as repulsion and hydrogen bonding, the distortion in the surface induced by adsorbing hydroxyls and water molecules is important. The competing direct intermolecular interactions and surface-mediated interactions lead to the interaction of hydroxyl groups over much longer distances compared with surface hydroxyls on SnO₂(110).

In order to investigate further the intermolecular interactions between adjacent adsorbates, monolayer adsorption on each surface was explored in Sec. IV C 2 in terms of binding energies and hydrogen bond lengths. It has been shown that on SnO₂(110) the hydrogen bond distance in \mathbf{a}_{slab} , $d(\text{H}_{\text{ads}}\text{O}_{\text{ads}})$, is unfavourable for strong hydrogen bonding between adjacent adsorbates. Consequently, the molecular adsorption mode is unstable in a configuration in which all sites are occupied by adsorbed water molecules, but can become stabilised in the mixed adsorption mode. Analysis of the water adsorption geometry and energetics has shown that the relative stability of water adsorption on SnO₂(110) is governed largely by the strength of the chemisorption and hydrogen bonds at the surface of the adsorbate-substrate system. On TiO₂(110), the interplay between chemisorption, hydrogen bonding and adsorbate-induced atomic displacements in the surface leads to a more complicated model of the the first layer of water on its surface.

The projected density of states of each surface in contact with a mixture of adsorbed water molecules and adsorbed hydroxyls sheds some light on the nature of the crystalline chemical bonds as well as on why adsorbed water has often been reported to be unstable on rutile SnO₂(110) (Sec. IV D). It has been shown that adsorbed H₂O states on TiO₂(110) hybridise strongly with the O-2*p* states of the surface, whereas a small amount of hybridisation is

seen when water is adsorbed on the SnO₂(110) surface, providing evidence in the electronic structure of the system to contribute as to why the molecular adsorption mode MM is unstable on SnO₂(110). The BH and TH states on SnO₂(110) hybridise strongly with the upper and lower VB, indicative of the stability of dissociative adsorption on this surface.

ACKNOWLEDGMENTS

This work made use of the high performance computing facilities of Imperial College London and, via our membership of the UK's HPC Materials Chemistry Consortium, which is funded by EPSRC (EP/L000202), of the facilities of HECToR and ARCHER, the UK's national high-performance computing service, which is funded by the Office of Science and Technology through EPSRC's High End Computing Programme.

-
- [1] T. Seiyama, A. Kato, K. Fujishi, and M. Nagatani, *Anal. Chem.* **34**, 1502 (1962).
 - [2] M. J. Madou and S. R. Morrison, *Chemical Sensing with Solid State Devices* (Academic Press, Boston MA, 1989) Chap. Chapters 1-3, p. 5.
 - [3] M. Batzill and U. Diebold, *Prog. in Surf. Sci.* **79**, 47 (2005).
 - [4] M. Haruta, N. Yamada, T. Kobayashi, and S. Iijima, *Journal of Catalysis* **115**, 301 (1989).
 - [5] K. J. Klabunde, L. Erickson, O. Koper, and R. Richards, *Review of nanoscale materials in chemistry: environmental applications* (American Chemical Society, 2010) Chap. Nanoscale materials in Chemistry: Environmental Applications, Chapter 1, pp. 1–13.
 - [6] M. Grätzel, *Nature* **414**, 338 (2001).
 - [7] A. Fujishima, *Nature* **238**, 37 (1972).
 - [8] R. H. Wilson, *J. Electrochem. Soc.* **127**, 228 (1980).
 - [9] P. Salvador, *Prog. in Surf. Sci.* **86**, 41 (2011).
 - [10] A. J. Bard and M. A. Fox, *Acc. Chem. Res.* **28**, 141 (1995).
 - [11] N. S. Lewis and D. G. Nocera, *Proc. Natl. Acad. Sci. U.S.A* **103**, 1572 (2006).
 - [12] E. Serrano, G. Rus, and J. Garcia-Martinez, *Renewable and Sustainable Energy Reviews* **13**, 2373 (2009).

- [13] V. E. Henrich and P. A. Cox, *The Surface Science of Metal Oxides* (Cambridge University Press, 1994) Chap. Geometric structure of metal-oxide surfaces, Chapter 2.3.3, pp. 42–49.
- [14] U. Diebold, J. Lehman, T. Mahmoud, M. Kuhn, G. Leonardelli, W. Hebenstreit, M. Schmid, and P. Varga, *Surface science* **411**, 137 (1998).
- [15] U. Diebold, J. Anderson, K. Ng, and D. Vanderbilt, *Physical review letters* **77**, 1322 (1996).
- [16] Typical surfaces contain a small amount of surface oxygen vacancies [86].
- [17] M. Batzill, K. Katsiev, and U. Diebold, *Surface Science* **529**, 295 (2003).
- [18] M. Batzill, *Sensors* **6**, 1345 (2006).
- [19] M. Batzill, K. Katsiev, J. M. Burst, U. Diebold, A. M. Chaka, and B. Delley, *Physical Review B* **72**, 165414 (2005).
- [20] Y. Duan, *Phys. Rev. B* **77**, 045332 (2008).
- [21] P. Ágoston and K. Albe, *Surface Science* **605**, 714 (2011).
- [22] M. Batzill and U. Diebold, *Progress in surface science* **79**, 47 (2005).
- [23] C. L. Pang, S. A. Haycock, H. Raza, P. J. Moller, and G. Thornton, *Phys. Rev. B* **62**, R7775 (2000).
- [24] M. Patel, G. Mallia, L. Liborio, and N. M. Harrison, *Phys. Rev. B* **86**, 045302 (2012).
- [25] R. A. Evarestov, A. V. Bandura, and E. V. Proskurov, *Phys. Stat. Sol.* **243**, 1823 (2006).
- [26] F. Labat, P. Baranek, C. Domain, C. Minot, and C. Adamo, *J. Chem. Phys.* **126**, 154703 (2007).
- [27] J. Muscat, A. Wander, and N. Harrison, *Chemical Physics Letters* **342**, 397 (2001).
- [28] M. Batzill, *Energy Environ. Sci.* **4**, 3275 (2011).
- [29] R. L. Kurtz, R. Stock-Bauer, T. E. Msdey, E. Romn, and J. D. Segovia, *Surface Science* **218**, 178 (1989).
- [30] V. E. Henrich, G. Dresselhaus, and H. J. Zeiger, *Solid State Communications* **24**, 623 (1977).
- [31] S. Eriksen, P. Naylor, and R. Egdell, *Spectrochimica Acta Part A: Molecular Spectroscopy* **43**, 1535 (1987).
- [32] M. B. Hugen Schmidt, L. Gamble, and C. T. Campbell, *Surface Science* **302**, 329 (1994).
- [33] M. A. Henderson, *Langmuir* **12**, 5093 (1996).
- [34] M. A. Henderson, *Surface Science* **355**, 151 (1996).
- [35] D. Brinkley, M. Dietrich, T. Engel, P. Farrall, G. Gantner, A. Schafer, and A. Szuchmacher, *Surface Science* **395**, 292 (1998).

- [36] R. Schaub, P. Thostrup, N. Lopez, E. Lægsgaard, I. Stensgaard, J. K. Nørskov, and F. Besenbacher, *Phys. Rev. Lett.* **87**, 266104 (2001).
- [37] I. M. Brookes, C. A. Muryn, and G. Thornton, *Phys. Rev. Lett.* **87**, 266103 (2001).
- [38] S. Krischok, O. Hofft, J. Gunster, J. Stultz, D. W. Goodman, and V. Kemper, *Surface Science* **495**, 8 (2001).
- [39] S. Wendt, R. Schaub, J. Matthiesen, E. K. Vestergaard, E. Wahlstrom, M. D. Rasmussen, P. Thostrup, L. Molina, E. Laegsgaard, I. Stensgaard, B. Hammer, and F. Besenbacher, *Surface Science* **598**, 226 (2005).
- [40] P. J. D. Lindan, N. M. Harrison, and M. J. Gillan, *Phys. Rev. Lett.* **80**, 762 (1998).
- [41] L. E. Walle, A. Borg, P. Uvdal, and A. Sandell, *Phys. Rev. B* **80**, 235436 (2009).
- [42] J. Goniakowski, S. Bouette-Russo, and C. Noguera, *Surface Science* **284**, 315 (1993).
- [43] J. Goniakowski and C. Noguera, *Surface Science* **330**, 337 (1995).
- [44] T. Bredow and K. Jug, *Surface Science* **327**, 398 (1995).
- [45] A. Fahmi and C. Minot, *Surface Science* **304**, 343 (1994).
- [46] J. Goniakowski, J. M. Holender, L. N. Kantorovich, M. J. Gillan, and J. A. White, *Phys. Rev. B* **53**, 957 (1996).
- [47] J. Goniakowski and M. J. Gillan, *Surface Science* **350**, 145 (1996).
- [48] M. Menetrey, A. Markovits, and C. Minot, *Surface Science* **524**, 49 (2003).
- [49] C. Zhang and P. J. D. Lindan, *J. Chem. Phys.* **118**, 4620 (2003).
- [50] D. Vogtenhuber, R. Podloucky, and J. Redinger, *Surface Science* **402-404**, 798 (1998).
- [51] M. Casarin, C. Maccato, and A. Vittadini, *Applied Surface Science* **142**, 196 (1999).
- [52] P. J. D. Lindan and C. Zhang, *Phys. Rev. B* **72**, 075439 (2005).
- [53] P. J. D. Lindan, J. Muscat, S. Bates, N. M. Harrison, and M. Gillan, *Faraday Discuss.* **106**, 135 (1997).
- [54] K. Sebbari, C. Domain, J. Roques, H. Perron, E. Simoni, and H. Catalette, *Surface Science* **605**, 1275 (2011).
- [55] V. A. Gercher and D. F. Cox, *Surf. Sci.* **322**, 177 (1995).
- [56] P. J. D. Lindan, *Chem. Phys. Lett.* **328**, 325 (2000).
- [57] S. P. Bates, *Surf. Sci.* **512**, 29 (2002).
- [58] A. V. Bandura, J. D. Kubicki, and J. O. Sofo, *J. Phys. Chem B* **112**, 11616 (2008).
- [59] K. R. Hahn, A. Tricoli, G. Santarossa, A. Vargas, and A. Baiker, *Langmuir* **28**, 1646 (2012).

- [60] R. Dovesi, V. R. Saunders, C. Roetti, R. Orlando, C. M. Zicovich-Wilson, F. Pascale, B. Cival-
leri, K. Doll, N. M. Harrison, I. J. Bush, P. D'Arco, and M. Llunell, *CRYSTAL09*, Università
di Torino (Torino, 2010).
- [61] R. Dovesi, B. Civalleri, E. Orlando, C. Roetti, and V. R. Saunders, *Reviews in Computational
Chemistry, Volume 21* (Wiley-VCH, John Wiley & Sons, Inc., 2005) Chap. Ab Initio Quantum
Simulation in Solid State Chemistry, pp. 1–126.
- [62] J. Muscat, N. M. Harrison, and G. Thornton, *Phys. Rev. B* **59**, 2320 (1999).
- [63] M. Habgood and N. Harrison, *Surf. Sci.* **602**, 1072 (2008).
- [64] J. Muscat, V. Swamy, and N. M. Harrison, *Phys. Rev. B* **65**, 224112 (2002).
- [65] D. Feller, *J. Comp. Chem.* **17**, 1571 (1996).
- [66] <https://bse.pnl.gov/bse/portal>.
- [67] G. S. Fanourgakis, G. K. Schenter, and S. S. Xantheas, *J. Chem. Phys.* **125**, 141102 (2006).
- [68] C. Pisani, R. Dovesi, and C. Roetti, *Hartree-Fock ab initio Treatment of Crystalline Systems*,
Lecture Notes in Chemistry, Vol. 48 (Springer Verlag, Heidelberg, 1988).
- [69] S. F. Boys and F. Bernardi, *Mol. Phys.* **19**, 553 (1970).
- [70] J. Scaranto, G. Mallia, and N. Harrison, *Comp. Mater. Sci.* **50**, 2080 (2011).
- [71] F. F. Sanches, G. Mallia, and N. M. Harrison, *MRS Online Proceedings Library* **1494** (2013),
10.1557/opl.2013.236.
- [72] R. D. Shannon, *Acta Crystallographica Section A* **32**, 751 (1976).
- [73] R. Wyckoff, *Crystal Structures*, 2nd. ed., Vol. 1 (Interscience, New York, 1964).
- [74] S. C. Abrahams and J. L. Bernstein, *J. Chem. Phys.* **55**, 3206 (1971).
- [75] T. Bredow, L. Giordano, F. Cinquini, and G. Pacchioni, *Phys. Rev. B* **70**, 035419 (2004).
- [76] T. He, J. L. Li, and G. W. Yang, *Appl. Mater. Interfaces* **4**, 2192 (2012).
- [77] P. D. Mitev, K. Hermansson, B. Montanari, and K. Refson, *Phys. Rev. B* **81**, 134303 (2010).
- [78] At monolayer coverage (1x1 unit cell), particularly strong interactions between neighbouring
terminal hydroxyls can be seen. The hydroxyls have tilted during the geometry optimisation
process in order to maximise the hydrogen bonding interactions and to avoid repulsive inter-
action between adjacent terminal hydroxyl groups. At lower coverage, this is not necessary.
The relative orientation of the hydroxyls is a consequence of the interactions occurring in the
system.

- [79] An interesting point to note is that the BE difference of 0.02 eV between dissociative and mixed adsorption modes is close in value to the thermal energy kT at room temperature, 0.025 eV, which makes it possible for thermal fluctuations in the system to affect the mode of adsorption on the surface.
- [80] The effect of the symmetry of the system on the BE has been documented previously and can be found in Ref. [24].
- [81] J. G. Traylor, H. G. Smith, R. M. Nicklow, and M. K. Wilkinson, *Phys. Rev. B* **3**, 3457 (1971).
- [82] G. A. Samara and P. S. Peercy, *Phys. Rev. B* **7**, 1131 (1973).
- [83] B. Montanari and N. M. Harrison, *Chem. Phys. Lett.* **364**, 528 (2002).
- [84] In both $\text{SnO}_2(110)$ and $\text{TiO}_2(110)$, there is some hybridisation of the VB states with the CB, and vice versa, which confirms the partially covalent character of Sn-O and Ti-O bonds.
- [85] C. Di Valentin, *The Journal of chemical physics* **127**, 154705 (2007).
- [86] U. Diebold, *Surface Science Reports* **48**, 53 (2003).